Weak catch bonds make strong networks

Mulla, Yuval; Avellaneda, Mario J.; Roland, Antoine; Baldauf, Lucia; Jung, Wonyeong; Kim, Taeyoon; Tans, Sander J.; Koenderink, Gijsje H.

DOI
10.1038/s41563-022-01288-0

Publication date
2022

Document Version
Final published version

Published in
Nature Materials

Citation (APA)
Mulla, Y., Avellaneda, M. J., Roland, A., Baldauf, L., Jung, W., Kim, T., Tans, S. J., & Koenderink, G. H. (2022). Weak catch bonds make strong networks. *Nature Materials*, *21*(9), 1019-1023. https://doi.org/10.1038/s41563-022-01288-0

nature materials

LETTERS

https://doi.org/10.1038/s41563-022-01288-0

Weak catch bonds make strong networks

Yuval Mulla[1,2], Mario J. Avellaneda[1,3], Antoine Roland[1], Lucia Baldauf[1,4], Wonyeong Jung[5,6], Taeyoon Kim[5] ✉, Sander J. Tans[1,4] ✉ and Gijsje H. Koenderink[1,4] ✉

Molecular catch bonds are ubiquitous in biology and essential for processes like leucocyte extravasion[1] and cellular mechanosensing[2]. Unlike normal (slip) bonds, catch bonds strengthen under tension. The current paradigm is that this feature provides 'strength on demand[3]', thus enabling cells to increase rigidity under stress[1,4–6]. However, catch bonds are often weaker than slip bonds because they have cryptic binding sites that are usually buried[7,8]. Here we show that catch bonds render reconstituted cytoskeletal actin networks stronger than slip bonds, even though the individual bonds are weaker. Simulations show that slip bonds remain trapped in stress-free areas, whereas weak binding allows catch bonds to mitigate crack initiation by moving to high-tension areas. This 'dissociation on demand' explains how cells combine mechanical strength with the adaptability required for shape change, and is relevant to diseases where catch bonding is compromised[7,9], including focal segmental glomerulosclerosis[10] caused by the α-actinin-4 mutant studied here. We surmise that catch bonds are the key to create life-like materials.

Here we exploit the actin-binding protein α-actinin-4 and its K225E point mutant, associated with the heritable disease kidney focal segmental glomerulosclerosis type 1 (ref. [10]), to identify the role of catch bonds in the mechanical properties of actin networks. Actin is a key determinant of cell mechanics, together with other cytoskeletal proteins. To isolate the role of catch bonds in actin mechanics, we reconstituted actin networks from purified components. We first characterized the binding affinity of the two protein variants for actin filaments in the absence of a mechanical load. Co-sedimentation of the crosslinkers with actin filaments revealed that the K255E mutant has a nearly tenfold higher affinity ($15.55 \pm 0.04\,\mu M^{-1}$) for actin than wild-type (WT) α-actinin-4 ($1.95 \pm 0.04\,\mu M^{-1}$; Fig. 1e and Extended Data Fig. 1). Fluorescence recovery after photobleaching measurements of crosslinker dissociation confirmed that WT α-actinin-4 has a substantially lower bond lifetime than the mutant (Extended Data Fig. 2), consistent with prior measurements in cells[11].

Based on crystal structures, it has previously been speculated that force activates a cryptic actin-binding site of α-actinin-4, thus behaving like a catch bond[12]. It was, furthermore, proposed that the cryptic actin-binding site is constitutively exposed by the K255E point mutation, increasing the binding affinity of α-actinin-4 but also abrogating its catch bond behaviour (Fig. 1a,b)[11,13]. To directly test this idea, we tethered single α-actinin-4 molecules to polystyrene beads via DNA handles, and probed their binding to fluorescently tagged actin filaments, which fully coated another set of beads (Fig. 1c). Using optical tweezers, we trapped an α-actinin-4-coated bead and an actin-coated bead, as verified by simultaneous fluorescence imaging (Extended Data Fig. 3b), and performed bead approach–retraction cycles. When we detected a force increase on retraction, which indicated a binding event, we subsequently maintained the tether at a preset force until the force suddenly dropped to zero and the beads separated (Fig. 1d), indicating forced crosslinker unbinding. The bond lifetime for WT α-actinin-4 showed a load dependence consistent with the predicted catch bond behaviour: short lifetimes at low loads, peaking at an intermediate load (around 4 pN), and decreasing for further increasing loads (Fig. 1f, red data). By contrast, the K255E point mutant showed slip bond behaviour, with a lifetime higher than the WT variant at lower loads, consistent with the biochemical data (Fig. 1e and Extended Data Figs. 1 and 2), and monotonically decreasing for increasing tensions (Fig. 1f, blue data). The single-molecule data provide direct proof of earlier speculations that α-actinin-4 forms weak catch bonds, whereas the K255E point mutant forms strong slip bonds[11,13].

The observation that catch bonds are weaker than slip bonds raises the question whether they also form weaker networks. To test the strength of crosslinked actin networks, we co-polymerized actin with either crosslinker between the cone and plate of a rheometer and linearly increased the mechanical load (shear stress) in time by rotating the cone until the network ruptured as the resulting network deformation (strain) is recorded (Fig. 2a). We first dissected the effect of the bond lifetime on network rupturing by measuring networks crosslinked by the mutant slip bonds at either high or low temperature (25 °C for low bond lifetime and 10 °C for high bond lifetime). The high temperature was chosen such that K255E had the same bond lifetime as the WT α-actinin-4 actin network at low temperature (Extended Data Fig. 4a–d). Consistent with intuition, we find that weaker linkers yield weaker networks (rupture stresses of 6.5 ± 0.5 and 8.1 ± 1.1 Pa at 25 and 10 °C, respectively; Fig. 2b). At the same time, the weaker networks are more deformable, meaning that they reach a much larger strain before rupturing ($129 \pm 10\%$ and $63 \pm 4\%$ at 25 and 10 °C, respectively; Fig. 2b). How about the catch bonds, which have a lower bond lifetime than the mutant slip bonds at the same temperature but exhibit a different load dependence? Strikingly, networks crosslinked by the α-actinin-4 catch bonds at 10 °C were not only more deformable than either of the slip bond networks (rupture strain of $221 \pm 16\%$) but also stronger (rupture stress of 24.5 ± 2.7 Pa; Fig. 2b).

How can catch bonds escape the tradeoff between strength and deformability that is inherent in normal (slip) bonds? To answer this question, we developed a minimal model where the crosslinked actin network was represented by an array of N reversible bonds sharing a load σ (Fig. 2c, Methods and Supplementary Information). We assumed nearest-neighbour load sharing (equation (2)), as it provides a simple yet accurate way to model crack

[1]Living Matter Department, AMOLF, Amsterdam, The Netherlands. [2]Institute for Biological Physics, University of Cologne, Cologne, Germany. [3]Institute of Science and Technology Austria, Klosterneuburg, Austria. [4]Department of Bionanoscience, Kavli Institute of Nanoscience Delft, Delft University of Technology, Delft, The Netherlands. [5]Weldon School of Biomedical Engineering, Purdue University, West Lafayette, IN, USA. [6]Ragon Institute of MGH, MIT and Harvard, Cambridge, MA, USA. ✉e-mail: kimty@purdue.edu; tans@amolf.nl; g.h.koenderink@tudelft.nl

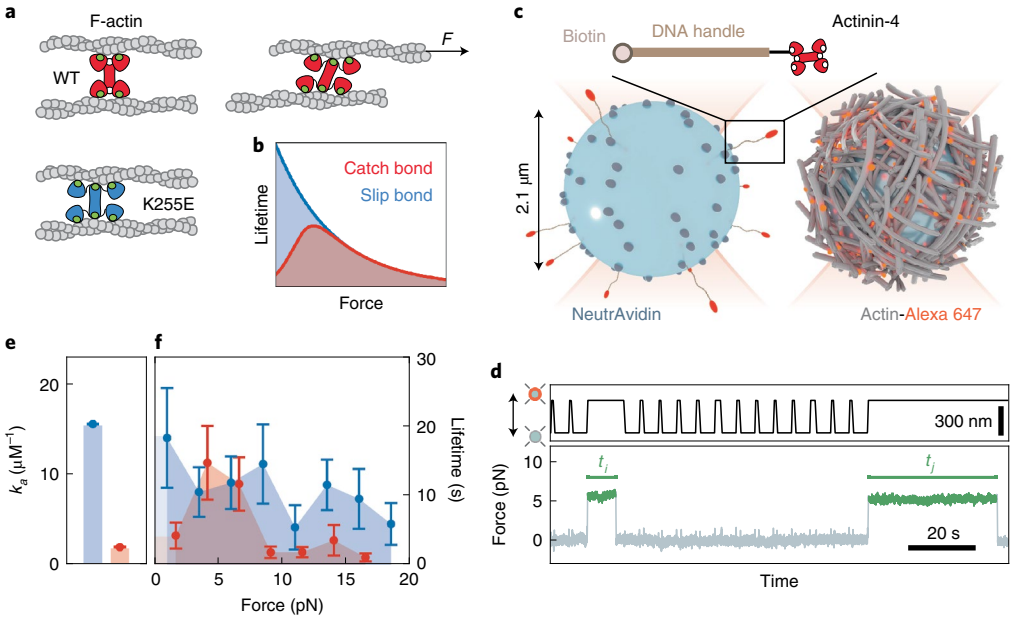

Fig. 1 | Single-molecule measurements of actin filament binding reveal catch bonding for WT α-actinin-4 but not the K255E mutant. a, Each monomer of the dimeric crosslinker α-actinin-4 (red) has two weak binding sites for actin filaments (green) and one strong binding site (white) that needs to be activated by force for the WT protein (red), whereas it is always exposed for the K255E mutant (blue). The force-induced shape transition is exaggerated for clarity. **b**, Lifetime of a catch bond first rises and then decreases with increasing force, whereas a constitutively active variant that acts as a regular slip bond shows a decreasing lifetime. The schematic shows a simplified limit in which the catch and slip bond lifetimes become equal at high force. **c**, Single-molecule force spectroscopy assay, where a crosslinker-coated bead and an actin-coated bead are trapped using optical tweezers. **d**, Example trace illustrating the approach-and-retract protocol to establish bonds between the crosslinkers and actin filaments (top). An increase in the force as retraction takes place indicates the presence of a tether (green), and the lifetime is measured until the instant the tether breaks (t_i, t_j; bottom). **e**, Actin association affinity k_a of α-actinin-4 (red) and K255E (blue) measured in a co-sedimentation assay. Data are presented as mean values ± standard error extracted from fitting the fraction of bound crosslinkers at six independent samples with different actin concentrations assuming Michaelis–Menten kinetics (Extended Data Fig. 1a–c). **f**, Average lifetime of tethers as a function of applied force, as measured by optical tweezers (as shown in **d**). The lifetime of WT α-actinin-4 (red) initially rises, peaks at a force of ~4 pN, and then decreases, as expected for a catch bond. The K255E mutant shows an overall decreasing lifetime, typical of a slip bond. Data are presented as mean values ± standard error. Numbers of data points per bin are 14, 13, 12, 18, 6, 4 and 4 for WT and 3, 9, 9, 10, 13, 13, 10 and 7 for the K255E mutant. Affinity and force spectroscopy data were obtained at 25 °C.

initiation in viscoelastic materials, which is the rate-limiting step of rupturing (Extended Data Fig. 5)[14,15]. We used idealized Bell–Evans force-dependent unbinding kinetics to capture the catch or slip bond behaviour (Fig. 1b and equation (1)), and allowed for unbound linkers to rebind at a random new location[16]. This bond turnover is proportional to network deformability (Supplementary Information). We chose our parameters in accordance with the force spectroscopy and biochemical data, such that the catch bonds are weaker at low force (Supplementary Table 1 lists all the parameters). Strikingly, the simulations also showed that weak catch bonds collectively make networks that are stronger than slip bond networks (rupturing at nearly twice the stress; Fig. 2d), yet more deformable (with tenfold more bond turnovers before rupturing; Fig. 2d). This difference persisted when including partially bound crosslinkers to account for the fact that α-actinin is a homodimer (Extended Data Fig. 6d and Supplementary Note 1). The model also confirmed the experimental observation that simply decreasing the bond lifetime while retaining a slip bond response results in weaker networks (Fig. 2d).

To identify the mechanism behind the remarkable mechanical advantage of catch bonds, we quantified the steady-state distributions of the load per individual crosslinker (Fig. 3a). At a given macroscopic load, the average force per bond was only slightly higher for the catch bonds compared with the slip bonds (0.241 ± 0.003 and 0.223 ± 0.001 (mean ± standard error), respectively). However, the distribution of forces for catch bonds was much narrower than for the slip bonds, meaning that slip bond networks contain substantially more bonds that bear high loads (Fig. 3a) and therefore fracture more readily. As bond load and bond–bond distance are directly proportional in our simple model (equation (2)), slip bond networks exhibit larger gaps than catch bond networks. To test whether the suppression of large gaps by catch bonding is a potential mechanism to prevent crack initiation, we ablated adjacent bonds and simulated the network stability as a function of gap size. Notably, gaps twice as large were required to rupture networks of catch bonds compared with slip bonds (Extended Data Fig. 5d). These findings suggest that catch bonds 'dissociate on demand' from low-stress areas owing to their shorter lifetime at lower loads, freeing up crosslinkers that can rebind in high-stress areas and hence prevent the initiation of cracks (Fig. 3b). Simulations also showed that the mechanical advantage of catch bonds over slip bonds was indeed lost when the catch bonds are immobile (Extended Data Fig. 6c).

As crosslinker rebinding is important for the mechanism, we next investigated how the mechanical advantage of catch bonding depends on the ratio between crosslinker binding and unbinding rate. We find that in the case of slow binding compared with unbinding, slip bonds provide stronger networks than catch bonds (Extended Data Fig. 7a): in this regime, catch-bond-induced dissociation strongly decreases the bound fraction, thereby weakening the network. By contrast, when binding is fast compared with unbinding, increased dissociation barely affects the bound fraction as crosslinkers rapidly rebind. Therefore, catch bonds provide

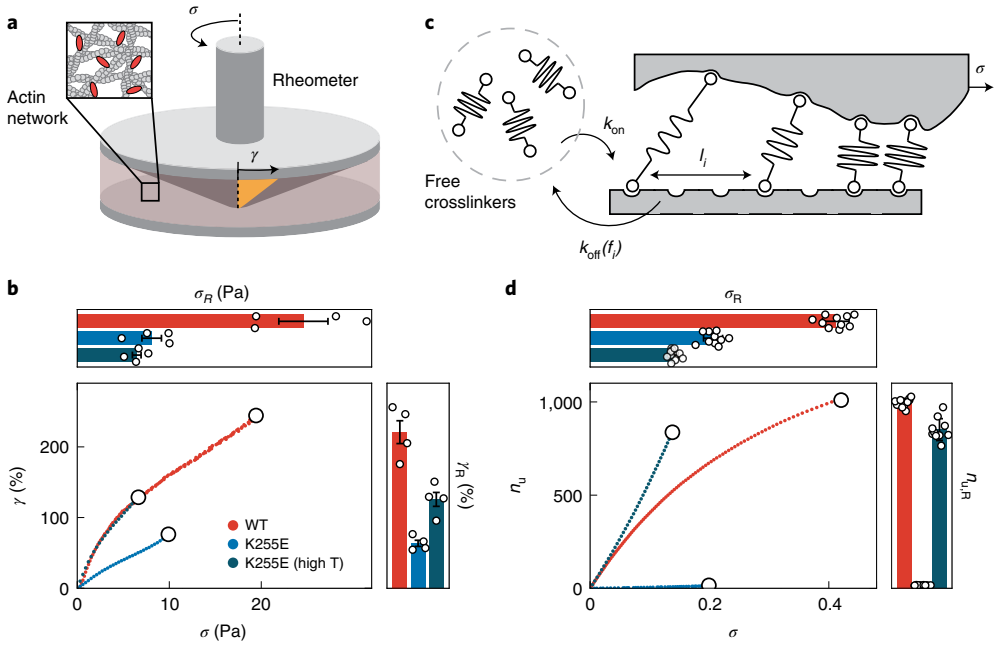

Fig. 2 | Catch bonds simultaneously enhance the mechanical strength and deformability of cytoskeletal actin networks. a, Scheme of rheology experiments to characterize actin network mechanics. We measure the shear deformation γ of actin networks crosslinked either with α-actinin-4 or with K255E by linearly increasing the shear stress σ in time with a stress rate of 2.0 mPa s^{-1}. **b**, Representative examples of shear strain γ as a function of shear stress σ for α-actinin-4 (red) and K255E (blue), both at 10 °C, as well as for K255E at an elevated temperature (25 °C, dark blue) where its lifetime matches that of WT α-actinin-4 at 10 °C (Extended Data Fig. 4c,d). The white circles indicate the rupture points (Methods). The top panel shows the average rupture stress and the right panel shows the average rupture strain for each condition. Data are presented as mean values ± standard error ($N = 4$ independent samples for each condition). **c**, Actin networks are modelled as 1D arrays of reversible linkers that stochastically exchange between a bound and freely diffusing state. The applied load (σ) linearly increases in time and is shared over all the bound linkers proportionally to the distance to the nearest neighbours l_i. **d**, Total number of unbinding events per bond n_u as a function of applied stress (Methods), showing the same crosslinker dependence as the rheology experiments. The data in the top and right panels are presented as mean values ± standard error ($N = 100$ independent simulations for each condition).

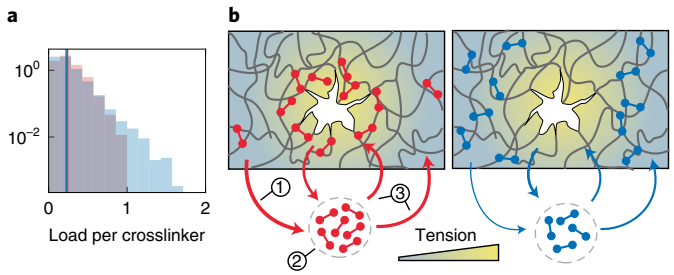

Fig. 3 | Minimal model suggest that catch bonds strengthen networks by redistributing to tense areas. a, Distribution of forces per bond f measured at the steady state in 1D simulations. The average bond force (vertical lines; 0.241 ± 0.003 and 0.223 ± 0.001 (mean ± standard error)) is larger for catch bonds (red) than for slip bonds (blue), but the force distribution of the former is much narrower: bonds carrying normalized forces higher than 1 are more than two orders of magnitude more probable for slip than for catch bonds. **b**, Self-assembly mechanism explaining the mechanical advantage of weak catch bonds (red, left) over strong slip bonds (blue, right). The thickness of the coloured arrows denotes the on and off rate of the linkers. Catch bond linkers in low-tension areas rapidly unbind (1), increasing the pool of unbound linkers (2). As a result, there is increased binding everywhere in the network (3), at the expense of only the linkers in low-tension areas. The net result is that the force distribution homogenizes, preventing crack initiation. By contrast, slip bonds preferentially localize in low-stress areas.

stronger networks only when the binding rate is fast compared with the unbinding rate (Extended Data Fig. 7a), which is the relevant situation for real actin networks crosslinked by α-actinin-4 (Extended Data Fig. 1d) and also appears to be the relevant regime in cells given the strong co-localization of α-actinin-4 with the actin cytoskeleton[8,11]. To experimentally test these predictions, we performed rupturing experiments on actin networks where we tuned the unbinding rate by changing the temperature. Consistent with the model's prediction, decreasing the temperature from 25 to 10 °C (and hence decreasing the unbinding rate) resulted in steeper increases in the rupture stress for the α-actinin-4 catch bonds than for the K255E slip bonds (Extended Data Fig. 7b).

Our model predicts that catch bonding triggered by network stress is key to explain the increased strength of the WT α-actinin-4 crosslinkers. To test whether the loads exerted on the network were indeed sufficient to activate the catch bonds, we determined the crosslinker-unbinding time from the network mechanics at different levels of shear stress, using a small oscillatory stress at different frequencies to measure the viscoelastic response time. This assay provides the characteristic network relaxation time, which is directly proportional to the crosslinker-unbinding time (Supplementary Note 2)[17]. The network relaxation time in the case of WT α-actinin-4 crosslinkers increased with the shear stress, followed by a decrease at the highest stress levels, consistent with catch bonding (Extended Data Fig. 4h). For the K255E crosslinkers, the stress relaxation time was larger than for the catch bonds at low shear stress but similar at high stress (Extended Data Fig. 4h). These findings confirm the single-molecule data (Fig. 1f) at the network level and show that macroscopically applied stresses above 5 Pa indeed activate strong binding for WT α-actinin-4, whereas the K255E mutant behaves like a conventional slip bond, being the strongest at small loads.

Our experiments and one-dimensional (1D) simulations together suggest that catch bonds strengthen actin networks by being able to

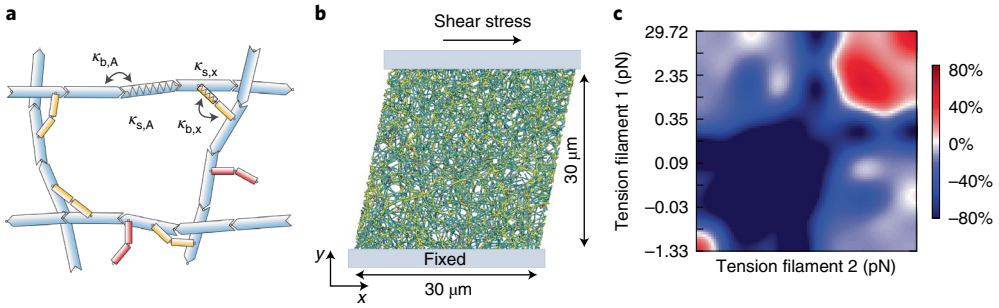

Fig. 4 | Detailed actin network simulations confirm catch-bond network strengthening via dissociation on demand. a, Schematic of actin network simulations. Actin filaments (F-actins, cyan) are simplified into serially connected cylindrical segments. Crosslinkers are simplified into two arm segments connected by elastic hinges. Crosslinkers binding to two F-actins to form a functional crosslink (yellow). Inactive crosslinkers bound to one F-actin (red). Bending (κ_b) and extensional (κ_s) stiffnesses govern the mechanical behaviours of these segments (Supplementary Table 2). **b**, Schematic showing how the network (30 × 30 × 1 µm) is deformed by linearly increasing the shear strain by fixing the bottom of the network and displacing the top in the +*x* direction. **c**, Ratio of catch and slip bond crosslinkers in colour as a function of tension in the two filaments they connect, derived from two simulations at 10 Pa stress (one with catch bonds and one with slip bonds). Colour scale: percentage relative enrichment of catch bonds over slip bonds bound between a pair of actin filaments for varying tensions on filament 1 (vertical axis) and filament 2 (horizontal axis). Specifically, the colour scale is defined as $\left(\left(\frac{n_{catch}}{n_{slip}} - 1\right) \times 100\%\right)$ for $n_{catch} > n_{slip}$ (shown in red) and $\left(-\left(\frac{n_{slip}}{n_{catch}} - 1\right) \times 100\%\right)$ for $n_{slip} > n_{catch}$ (shown in blue), where n_{catch} and n_{slip} are the number of respective catch and slip bond linkers connecting two filaments. Compression is reported as negative tension. Here 10 × 10 tension bins are used, and the distribution was smoothed using bicubic interpolation. The tension spacing is chosen such that each bin includes 10% of the filaments (Extended Data Fig. 8b), is the same for the *x* and *y* axes, and is only displayed on the *y* axis for aesthetic reasons. The simulations show that catch bonding linkers preferentially connect two high-tension filaments, whereas slip bonding linkers are enriched on low-tension filament pairs.

redistribute to tense regions under load. However, these simple simulations lack an explicit polymer network. We, therefore, decided to probe bond redistribution by realistic three-dimensional simulations of actin networks[18–21] (Fig. 4a, Methods, Supplementary Note 3 and Supplementary Table 2). These simulations contain explicit filaments and capture the main features of actin network mechanics and allow for microscopic force measurements that are not experimentally tractable. We simulated strain ramps on networks connected by either catch or slip bonds (Supplementary Video 1, Fig. 4b and Extended Data Fig. 8a). It is well known that stress is mostly carried by a small subset of tense filaments in actin networks[20]; therefore, we analysed how effective catch and slip bond crosslinkers were at connecting these tense filaments. Strikingly, we found that catch bonds formed up to 80% more links between pairs of highly tensed filaments than slip bonds (Fig. 4c and Extended Data Fig. 8e,f), despite binding less on average (Extended Data Fig. 8c). Furthermore, this preferential binding to stressed actin filaments increased as the bulk shear stress was raised (Supplementary Video 2). These findings directly verify the catch bond redistribution to high-stress areas as predicted by the 1D model.

Our work reveals a new role for catch bonds in the cytoskeleton, namely, to simultaneously increase its mechanical strength and its deformability. Contrary to the common intuition that catch bonds provide strength on demand, our model shows that they make strong networks because dissociation on demand enables them to redistribute to tense areas and thus postpone crack initiation. This mechanism probably also applies to living cells, as α-actinin-4 is mobile inside the actin cortex and was recently observed to increase its bond lifetime on mechanical stress in living cells[22]. Force sensors for α-actinin-4 analogous to those available for other proteins[23] could be developed and resolved with single-molecule resolution to directly visualize the load-dependent redistribution for catch and slip bonds in both reconstituted actin networks and living cells.

Our findings also suggest a molecular mechanism to explain the low mechanical stability of kidney cells in patients afflicted by heritable disease kidney focal segmental glomerulosclerosis type 1, where α-actinin-4 carries the point mutation K255E and is known to cause podocyte fragility[10,24]. A similar mechanism may possibly apply to other diseases where the loss of catch bonding leads to tissue failure, such as von Willebrand disease type 2B (refs. [7,9]). In this work, we focused on the implications of catch bonds for network strength, but the generality of our model implies that this same mechanism can also apply to catch bonds in cell–matrix and cell–cell adhesions[1,2], as dissociation on demand reduces friction and simultaneously minimizes the risk of complete cell detachment. Therefore, our results suggest that catch bonds are widespread in the cytoskeleton and at cellular interfaces to break this deformability/strength tradeoff, and it would be interesting to investigate force-dependent binding of more crosslinkers and adhesins, such as filamin and immunoglobulin-like cell adhesion molecules. Finally, our findings offer a cell-inspired route to create hydrogel materials that are strong yet sufficiently deformable for applications in regenerative medicine[25]. Recent years have seen a surge in theoretical and experimental work in the polymer community to create tougher hydrogels, for instance, by the inclusion of stiff elements into the hydrogel[26–28]. However, these approaches have largely focused on preventing crack propagation rather than crack initiation. Preventing crack propagation works well to absorb a finite amount of mechanical energy but offers limited advantage in the case of constant stress. For future work, it would be interesting to combine mitigation strategies for both crack initiation and propagation. Synthetic analogues of catch bonds have recently been discovered and provide an excellent starting point towards highly dynamic yet strong biomimetic materials[29,30].

Online content

Any methods, additional references, Nature Research reporting summaries, source data, extended data, supplementary information, acknowledgements, peer review information; details of author contributions and competing interests; and statements of data and code availability are available at https://doi.org/10.1038/s41563-022-01288-0.

Received: 8 September 2020; Accepted: 11 May 2022;
Published online: 25 August 2022

References

1. Marshall, B. T. et al. Direct observation of catch bonds involving cell-adhesion molecules. *Nature* **423**, 190–193 (2003).
2. Liu, B., Chen, W., Evavold, B. D. & Zhu, C. Accumulation of dynamic catch bonds between TCR and agonist peptide-MHC triggers T cell signaling. *Cell* **157**, 357–368 (2014).
3. Mbanga, B. L., Iyer, B. V. S., Yashin, V. V. & Balazs, A. C. Tuning the mechanical properties of polymer-grafted nanoparticle networks through the use of biomimetic catch bonds. *Macromolecules* **49**, 1353–1361 (2016).
4. Thomas, W. E., Trintchina, E., Forero, M., Vogel, V. & Sokurenko, E. V. Bacterial adhesion to target cells enhanced by shear force. *Cell* **109**, 913–923 (2002).
5. Huang, D. L., Bax, N. A., Buckley, C. D., Weis, W. I. & Dunn, A. R. Vinculin forms a directionally asymmetric catch bond with F-actin. *Science* **357**, 703–706 (2017).
6. Petrie, R. J., Koo, H. & Yamada, K. M. Generation of compartmentalized pressure by a nuclear piston governs cell motility in a 3D matrix. *Science* **345**, 1062–1065 (2014).
7. Yago, T. et al. Platelet glycoprotein Ibα forms catch bonds with human WT vWF but not with type 2B von Willebrand disease vWF. *J. Clin. Invest.* **118**, 3195–3207 (2008).
8. Luo, T., Mohan, K., Iglesias, P. A. & Robinson, D. N. Molecular mechanisms of cellular mechanosensing. *Nat. Mater.* **12**, 1064–1071 (2013).
9. Kim, J., Zhang, C.-Z., Zhang, X. & Springer, T. A. A mechanically stabilized receptor–ligand flex-bond important in the vasculature. *Nature* **466**, 992–995 (2010).
10. Feng, D., DuMontier, C. & Pollak, M. R. Mechanical challenges and cytoskeletal impairments in focal segmental glomerulosclerosis. *Am. J. Physiol. Renal Physiol.* **314**, F921–F925 (2018).
11. Ehrlicher, A. J. et al. Alpha-actinin binding kinetics modulate cellular dynamics and force generation. *Proc. Natl Acad. Sci. USA* **112**, 6619–6624 (2015).
12. Ribeiro, E. D. A. et al. The structure and regulation of human muscle α-actinin. *Cell* **159**, 1447–1460 (2014).
13. Yao, N. Y. et al. Stress-enhanced gelation: a dynamic nonlinearity of elasticity. *Phys. Rev. Lett.* **110**, 018103 (2013).
14. Mulla, Y., Oliveri, G., Overvelde, J. T. B. & Koenderink, G. H. Crack initiation in viscoelastic materials. *Phys. Rev. Lett.* **120**, 268002 (2018).
15. Mulla, Y. & Koenderink, G. H. Crosslinker mobility weakens transient polymer networks. *Phys. Rev. E* **98**, 062503 (2018).
16. Mulla, Y., Wierenga, H., Alkemade, C., ten Wolde, P. R. & Koenderink, G. H. Frustrated binding of biopolymer crosslinkers. *Soft Matter* **15**, 3036–3042 (2019).
17. Mulla, Y., Mackintosh, F. C. & Koenderink, G. H. Origin of slow stress relaxation in the cytoskeleton. *Phys. Rev. Lett.* **122**, 218102 (2019).
18. Jung, W., Murrell, M. P. & Kim, T. F-actin cross-linking enhances the stability of force generation in disordered actomyosin networks. *Comp. Part. Mech.* **2**, 317–327 (2015).
19. Kim, T. Determinants of contractile forces generated in disorganized actomyosin bundles. *Biomech. Model. Mechanobiol.* **14**, 345–355 (2014).
20. Kim, T., Hwang, W., Lee, H. & Kamm, R. D. Computational analysis of viscoelastic properties of crosslinked actin networks. *PLoS Comput. Biol.* **5**, e1000439 (2009).
21. Mak, M., Zaman, M. H., Kamm, R. D. & Kim, T. Interplay of active processes modulates tension and drives phase transition in self-renewing, motor-driven cytoskeletal networks. *Nat. Commun.* **7**, 10323 (2016).
22. Hosseini, K., Sbosny, L., Poser, I. & Fischer-Friedrich, E. Binding dynamics of à-actinin-4 in dependence of actin cortex tension. *Biophys. J.* **119**, P1091–1107 (2020).
23. Grashoff, C. et al. Measuring mechanical tension across vinculin reveals regulation of focal adhesion dynamics. *Nature* **466**, 263–266 (2010).
24. Feng, D. et al. Disease-causing mutation in α-actinin-4 promotes podocyte detachment through maladaptation to periodic stretch. *Proc. Natl Acad. Sci. USA* **115**, 1517–1522 (2018).
25. Rosales, A. M. & Anseth, K. S. The design of reversible hydrogels to capture extracellular matrix dynamics. *Nat. Rev. Mater.* **1**, 15012 (2016).
26. Rivera, J. et al. Toughening mechanisms of the elytra of the diabolical ironclad beetle. *Nature* **586**, 543–548 (2020).
27. Wang, C. et al. Visible-light-assisted multimechanism design for one-step engineering tough hydrogels in seconds. *Nat. Commun.* **11**, 4694 (2020).
28. Zhang, L., Bailey, J. B., Subramanian, R. H., Groisman, A. & Tezcan, F. A. Hyperexpandable, self-healing macromolecular crystals with integrated polymer networks. *Nature* **557**, 86–91 (2018).
29. Garcia-Manyes, S., Liang, J., Szoszkiewicz, R., Kuo, T.-L. & Fernández, J. M. Force-activated reactivity switch in a bimolecular chemical reaction. *Nat. Chem.* **1**, 236–242 (2009).
30. Dansuk, K. C. & Keten, S. Self-strengthening biphasic nanoparticle assemblies with intrinsic catch bonds. *Nat. Commun.* **12**, 85 (2021).

Methods

Minimal 1D crosslinker model. To investigate the effect of molecular catch bonding on the strength of cytoskeletal filament networks, we use a computational model we recently developed to predict the failure of transient networks[14,15], using a Gillespie algorithm to model stochastic linker binding and unbinding. The detailed motivation behind the design of the model, including a discussion of its assumptions and limitations, are presented in Supplementary Note 1. We consider a 1D model of N linkers that share an externally applied load σ (Fig. 2c). We model the effect of force f on the unbinding rate k_{off} (inverse bond lifetime) of a bound linker i using the Bell–Evans equation[31]:

$$k_{\mathrm{off},i}(f_i) = \left(k_{\mathrm{off},0}^{\mathrm{catch}} \times e^{\frac{-f_i}{f_{1/e}^{\mathrm{catch}}}}\right) + \left(k_{\mathrm{off},0}^{\mathrm{slip}} \times e^{\frac{f_i}{f_{1/e}^{\mathrm{slip}}}}\right), \quad (1)$$

The first exponent models the catching of the weakly bound state, whereas the second exponent models the slipping of the force-activated state. We compare catch bonds with slip bonds, which do not require force activation for strong binding ($k_{\mathrm{off},0}^{\mathrm{catch}} = 0$), keeping all the other parameters identical (Supplementary Table 1 provides the full list of parameters used for each simulation). To account for mobility by random diffusion of linkers after unbinding, we allow for unbound linkers to rebind at a random new location[15,16]. As the actin concentration is much larger than the crosslinker concentration both in our reconstituted networks (48.00 versus 0.48 μM, respectively) and in living cells (~100 versus ~1 μM, respectively[32]), we consider tenfold more binding sites than crosslinkers to prevent competition for actin-binding sites. For control simulations where the linkers are immobile (Extended Data Fig. 6c), we only allow for rebinding in the same place where the crosslinkers are unbound[14].

It is known that stressed networks connected by reversible bonds exhibit spontaneous crack initiation and propagation due to inhomogeneous load sharing[33]. We reproduce this rupturing behaviour using a minimal model where the force per linker f_i is proportional to the global applied stress and the distance between its nearest neighbours on both sides l_i in one dimension (Fig. 2c).

$$f_i = \frac{l_i}{\sum_i l_i} \times \sigma \times N \quad (2)$$

The stress is normalized by the force per crosslinker, such that $\frac{\sigma \times N}{f_{1/e}^{\mathrm{slip}}} = \sum_i f_i$. Time is normalized by the binding rate as we keep $k_{on} = 1$. We use a periodic boundary condition to prevent edge effects. We initialize networks by randomly placing $N \times \frac{k_{on}}{k_{on}+k_{off,0}}$ linkers (Supplementary Table 1). Supplementary Note 1 and Extended Data Fig. 6a,b contain a more detailed discussion of the effect of network size.

Actin network simulations. We employed an agent-based computational model based on Brownian dynamics[34–37]. In this model, the actin filaments (F-actin) and crosslinkers are simplified by cylindrical segments (Fig. 4a). The motion of the cylindrical segments is determined by the Langevin equation. Bending and extensional forces maintain angles and distances formed by the cylindrical segments near their equilibrium values, respectively. A repulsive force represents volume-exclusion effects between overlapping F-actins. The details of the model are explained in Supplementary Note 3, and the parameter values are listed in Supplementary Table 2. We create a crosslinked actin network in a three-dimensional thin rectangular domain (30 × 30 × 1 μm) with a periodic boundary condition only in the x direction (Fig. 4b). The network is spontaneously assembled by dynamic events occurring on F-actins and crosslinkers; F-actin is formed by nucleation and polymerization events, and crosslinkers bind to elongating F-actin to form crosslinking points. The average filament length is ~12 μm. It is assumed that crosslinkers unbind from F-actins at a force-dependent rate; the unbinding rate follows either the slip or catch bond behaviour. After unbinding from one F-actin, crosslinkers also unbind quickly from the other F-actin, disappear and then appear in a different location whose distance is within 5 μm from the unbinding location. During network assembly, all the crosslinkers are assumed to behave as slip bonds. After network formation, the network is deformed by applying a shear strain that linearly increases at a rate of 0.001 s^{-1}. These simulations are performed with either slip or catch bond crosslinkers. The corresponding shear stress acting on the network at each strain level is measured. During shear deformation, we measure tensile forces acting on F-actins and analyse how crosslinkers are redistributed on pairs of filaments depending on tensile forces. As these simulations are strain controlled, network yielding does not display a sudden divergence of strain. Instead, the yielding points were determined as the first data point in which network stress decreases ($d\sigma/dt < 0$). As the simulated stress/strain curves are noisy (Extended Data Fig. 8a), we convoluted the raw curves with a 60-data-point time window before determining the rupture point.

Protein purification. Human WT α-actinin-4 and its K255E point mutant were purified according to another study[38]. Briefly, *Escherichia coli* cells were transformed to express recombinant crosslinkers with a His6 tag. Induction was performed with 500 μM isopropyl β-D-1-thiogalactopyranoside for 8 h at 25 °C. After centrifugation at 6,000*g* for 15 min, the cells were resuspended in 20 mM NaCl, 5 mg ml^{-1} lysozyme and 20 mM HEPES at pH 7.8. The cells were lysed by a freeze–thaw cycle and the lysate was centrifuged at 20,000*g* for 30 min. The recombinant proteins were purified from the supernatant using a QIAGEN nickel column that was first washed with 20 bed volumes of 500 mM NaCl, 25 mM imidazole and 20 mM HEPES at pH 7.8. The recombinant proteins were eluted with ten bed volumes of 500 mM NaCl, 500 mM imidazole and 20 mM HEPES at pH 7.8, concentrated using Centricon filters (Millipore), and purified by gel filtration in 150 mM NaCl, 20 mM HEPES at pH 7.8 and 10 mM dithiothreitol (DTT). Actin was labelled using an Alexa Fluor labelling kit purchased from Thermo Fisher and biotin-actin was purchased from Cytoskeleton.

To ensure we compare α-actinin-4 and K255E at the same concentration in all our assays, we determined the ratio of the protein stock concentrations by measuring the intensity of the protein bands on an sodium dodecyl sulfate–polyacrylamide gel electrophoresis (SDS-PAGE) gel. We chose this method because unlike ultraviolet–visible spectrophotometry, it specifically measures the protein of interest and excludes the contribution of any contaminants. The proteins were cysteine labelled using maleimide-activated Oregon Green at a ratio of five fluorophores for every crosslinker at room temperature for 1 h. The labelled proteins were separated from free dye molecules by gel filtration using a Superdex 200 column (GE Healthcare)[38].

Actin was purified from rabbit psoas skeletal muscle as described elsewhere[16], including the gel filtration step to remove oligomers. The concentration was determined by measuring the optical absorbance at 280 nm. Aliquots were snap frozen and stored at −80 °C in G-buffer (2.0 mM tris-hydrochloride at pH 8.0, 0.2 mM disodium adenosine triphosphate, 0.2 mM calcium chloride and 0.2 mM DTT) to prevent polymerization. After thawing, we stored G-actin stock samples overnight at 4 °C. The next day, we spun the sample at 120,000*g* to remove any remaining aggregates. The supernatants were stored at 4 °C and used within seven days. We polymerized actin at a concentration of 48 μM (2 mg ml^{-1}) in an F-buffer consisting of 50.0 mM KCl, 20.0 mM imidazole at pH 7.4, 2.0 mM $MgCl_2$, 1.0 mM DTT and 0.5 mM MgATP in the presence of a crosslinker at a concentration of 0.48 μM (corresponding to a molar ratio of 1/100 crosslinker/actin and on average around one crosslinker for every 0.5 μm length of actin filament). We verified that the networks under these conditions are isotropic and spatially uniform by confocal fluorescence imaging (Extended Data Fig. 9). Unless otherwise mentioned, all the chemicals were purchased from Sigma-Aldrich.

SDS-PAGE gel protocol and quantification. SDS-PAGE gels were used to characterize and quantify the purified proteins. In all the cases, 20 μl sample was mixed with 20 μl InstantBlue and boiled at 95 °C for 5 min in a closed Eppendorf vial. Then, 30 μl of this solution was loaded onto a 4–15% Mini-PROTEAN TGX precast protein gel with ten wells of 30 μl. Gels were run for 30 min at 200 V, washed with Milli-Q water, stained overnight with InstantBlue and washed three times with tap water. Band intensities were quantified using ImageJ (v. 1.52i) software[39]. Background correction was applied to all the band intensities by subtracting the average intensity of a region adjacent to the band of interest.

Fluorescence recovery after photobleaching. The bond lifetime of bound crosslinkers was measured via fluorescence recovery after photobleaching using a Nikon A1 confocal microscope with a perfect focus system (×100, numerical aperture of 1.40, oil-immersion objective) and 100 mW, 488 nm argon-ion laser. We acquired ten images to determine the baseline fluorescence and then performed photobleaching by increasing the laser power such that 50–70% of the fluorescence intensity was bleached in 0.5 s. We then tracked the fluorescence recovery with a low-intensity beam during a period of approximately five times the typical recovery time, with a sampling rate that halved every ten frames, starting with 10 fps. During imaging, the exposure time was kept fixed at 0.1 s per frame. We bleached a circular area of 2 μm radius and used an equally sized area as a reference. The laser intensity during imaging was chosen such that the reference intensity dropped less than 5% during the recovery phase. To extract a timescale for fluorescence recovery, τ_{FRAP}, the time-dependent intensity normalized by the intensity of the reference area was fitted with a single exponential function: $I(t)/I_{ref} = 1 - I/I_0 \times e^{-t/\tau_{FRAP}}$, where I_0 is the intensity directly after bleaching[16].

Co-sedimentation assay. A volume of 25 μl monomeric actin (G-actin) at increasing concentrations was co-polymerized with either α-actinin-4 or K255E in F-buffer at room temperature, keeping the crosslinker concentration constant (0.1 μM). After 2 h of polymerization, the actin network together with the bound crosslinkers was spun down at 120,000*g*. Afterwards, 20 μl was gently pipetted from the supernatant and run on an SDS-PAGE gel as described above. The fraction of bound linkers φ_{bound} was determined by subtracting and normalizing the crosslinker band intensity I at a particular actin concentration by band intensity I_0 in the absence of actin using ImageJ software: $\varphi_{bound} = \frac{I - I_0}{I_0}$.

Rheology. Rheology was performed using a stress-controlled Kinexus Malvern Pro rheometer with a stainless-steel cone–plate geometry having a radius of 20 mm and a cone angle of 1°. We loaded 40 μl samples of actin monomers, directly after mixing with either α-actinin-4 or K255E and F-buffer, onto the bottom plate and

quickly lowered the cone. A thin layer of Fluka mineral oil type A was added around the edge to prevent solvent evaporation, and the sample was closed off with a hood to prevent any effects of air flow. Actin polymerization was followed by applying a small oscillatory shear with a strain amplitude of 0.5% and a frequency of 0.5 Hz. After 2 h of polymerization, the elastic shear modulus G' and viscous shear modulus G'' were measured as a function of frequency by performing small-amplitude oscillatory shear measurements at frequencies between 0.01 and 10.00 Hz, taking 30 logarithmically spaced data points. Frequencies above 10 Hz could not be accessed as inertial effects from the rheometer started to dominate the rheological response of the actin network. We used an analytical biopolymer network model to analyse the frequency-dependent viscous shear modulus, $G'(\omega)$, to extract the crosslinker lifetime in the absence of stress[16,40]. The model is based on the force-extension curve of a semiflexible filament, and uses mean-field arguments to calculate the mechanical properties of the network from single-filament fluctuations:

$$G' \propto \left(\chi' + \alpha'(\omega)/[(\chi' + \alpha'(\omega))^2 + (\chi'' + \alpha''(\omega))^2\right], \tag{3}$$

$$G'' \propto \left(\chi'' + \alpha''(\omega)/[(\chi' + \alpha'(\omega))^2 + (\chi'' + \alpha''(\omega))^2\right], \tag{4}$$

where χ describes the viscous-drag-limiting transverse filament fluctuations.

$$\chi' = \frac{0.0072}{4\sqrt{2}} \frac{\left[\begin{array}{l} 2\tan^{-1}\left(1+\frac{\sqrt{2}}{\sqrt{\frac{\omega}{\omega_{\mathrm{fluid}}}}}\right) - 2\tan^{-1}\left(1-\frac{\sqrt{2}}{\sqrt{\frac{\omega}{\omega_{\mathrm{fluid}}}}}\right) \\ +\log\left(1+\frac{\omega_{\mathrm{fluid}}}{\omega}-\frac{\sqrt{2}}{\sqrt{\frac{\omega}{\omega_{\mathrm{fluid}}}}}\right) - \log\left(1+\frac{\omega_{\mathrm{fluid}}}{\omega}+\frac{\sqrt{2}}{\sqrt{\frac{\omega}{\omega_{\mathrm{fluid}}}}}\right) \end{array}\right]}{\sqrt{\frac{\omega}{\omega_{\mathrm{fluid}}}}} \tag{5}$$

$$\chi'' = \frac{0.0072}{4\sqrt{2}} \frac{\left[\begin{array}{l} 2\tan^{-1}\left(1+\frac{\sqrt{2}}{\sqrt{\frac{\omega}{\omega_{\mathrm{fluid}}}}}\right) - 2\tan^{-1}\left(1-\frac{\sqrt{2}}{\sqrt{\frac{\omega}{\omega_{\mathrm{fluid}}}}}\right) \\ -\log\left(1+\frac{\omega_{\mathrm{fluid}}}{\omega}-\frac{\sqrt{2}}{\sqrt{\frac{\omega}{\omega_{\mathrm{fluid}}}}}\right) + \log\left(1+\frac{\omega_{\mathrm{fluid}}}{\omega}+\frac{\sqrt{2}}{\sqrt{\frac{\omega}{\omega_{\mathrm{fluid}}}}}\right) \end{array}\right]}{\sqrt{\frac{\omega}{\omega_{\mathrm{fluid}}}}} \tag{6}$$

Here ω_{fluid} is the timescale of the fluid drag, which is typically on the order of 100 Hz for actin networks, depending on the fluid viscosity as well as crosslinker and actin concentrations[16], whereas α describes the effect of the crosslinker-limiting transverse filament fluctuations.

$$\alpha' = \frac{1}{\pi^4}\sum_{n=1}^{N}\frac{n^4}{n^8 + (\omega/\omega_{\mathrm{off}})^2} \tag{7}$$

$$\alpha'' = \frac{1}{\pi^4}\sum_{n=1}^{N}\frac{\frac{\omega}{\omega_{\mathrm{off}}}}{n^8 + \left(\frac{\omega}{\omega_{\mathrm{off},0}}\right)^2} \tag{8}$$

Here N is the number of crosslinkers per filament and $\omega_{\mathrm{off},0}$ is the off rate of the crosslinker in the absence of force, which we can numerically extract by fitting $G'(\omega)$ to equations (4)–(7) (Extended Data Fig. 4d). Having characterized the linear rheology, we finally performed a rupture experiment by linearly increasing the stress in time at a constant loading rate (2 mPa s^{-1}) until the network ruptured. To unambiguously identify the rupture point, we measured the differential elastic modulus K' of the network as a function of stress by superposing small stress oscillations on top of the stress ramp. The rate of 2 mPa s^{-1} was chosen because it was sufficiently slow to reliably measure K' at every stress level, whereas it was sufficiently fast to prevent network aging effects during the stress ramp. We observed stress stiffening above a threshold stress, consistent with prior literature[17], followed by a rapid drop in K' that signals rupture. We defined the rupture point as the stress value where K' peaked (Extended Data Fig. 4e). This approach allowed us to simultaneously identify the rupture stress and rupture strain (Fig. 2c).

To obtain the bond lifetime in the presence of stress, we use a recent extension[17] of the biopolymer network model described above that takes into account stress-induced network stiffening. Briefly, we superposed an oscillatory stress on top of a constant mechanical load to measure the differential storage modulus $K'(\sigma,\omega)$ over a wide range of frequencies ($0.01 < \omega < 10.00$ Hz) and stresses ($0.1 < \sigma < 8.0$ Pa) and then fitted the data to the following equation:

$$K' \propto \frac{(1 + (\sigma + \sigma_{0,\mathrm{tr}}))^{\frac{3}{2}}}{1 + \sqrt{\omega_{\mathrm{off}}(\sigma) + \omega}}, \tag{9}$$

where $\omega_{\mathrm{off}}(\sigma)$ is the stress-dependent crosslinker-unbinding frequency and $\sigma_{0,\mathrm{tr}}$ is the critical stress for stress stiffening in the fast limit where crosslinkers have not had time to unbind (Extended Data Fig. 4f–i).

To test whether wall slip contributes to fracturing, we performed control experiments where we fractured actin networks in the absence or presence of a polylysine-coated glass plate adhered to the bottom and top plates of the rheometer. Polylysine is known to strongly bind actin networks, but neither rupture strain nor rupture stress substantially changed upon this surface modification (Extended Data Fig. 10)—showing that fracturing occurred within the network and was not due to wall slip.

Generation of single-molecule constructs. Both WT α-actinin-4 and the K255E mutant were modified to include a ybbR tag (DSLEFIASKLA)[41] right after the His6 tag. Purified proteins were coupled to co-enzyme A–modified DNA oligonucleotides (20 nucleotides long) using a phosphopantetheinyl transferase (SFP synthase)-mediated reaction[41]. A protein-to-DNA molar ratio of 10:1 ensured that only one monomer was coupled to the DNA, as evidenced by the SDS-PAGE analysis (Extended Data Fig. 3a). Next, 2.5-kilo-base-pair DNA tethers were amplified via polymerase chain reaction from the pUC19 plasmid (New England Biolabs) with a 5′-biotinylated primer on one side and a 5′-phosphoprimer on the other side. Purification was done with the QIAquick polymerase chain reaction purification kit (QIAGEN). The phosphorylated strand was digested using λ-exonuclease (New England Biolabs) for 2 h at 37 °C and purified using an Amicon 30 kDa molecular weight cutoff filter (Merck). Deep Vent exo-DNA polymerase (New England Biolabs) and an upstream primer 20 nucleotides more than the phosphoprimer from the polymerase chain reaction was used to fill up the second DNA strand, creating a 20 nucleotide overhang[42]. This overhang is complementary to the 20 oligonucleotide sequence coupled to the proteins. The generated DNA tether was then ligated to the DNA–protein hybrid by overnight incubation with T4 ligase (New England Biolabs) at room temperature. The stock sample was flash frozen and stored at −80 °C, and small aliquots were stored at 4 °C for a maximum of one week.

Preparation of actin-coated and crosslinker-coated beads. Unlabelled actin monomers were mixed with biotinylated monomers and fluorescent monomers labelled with Alexa Fluor 647 in a molar ratio of 8:1:1 and polymerized into filaments in 1 ml F-buffer at a concentration of 2 μM for 2 h. Next, these filaments were mixed with 4 μl of 2.4 μM NeutrAvidin-coated beads (NVP-20-5 with a diameter of 2.1 μm; Spherotech) and incubated for 15 min to couple the filaments to the beads. The actin-coated beads were separated from the unbound actin filaments by centrifuging thrice at 1,000*g* for 2 min. After every round, 800 μl supernatant was discarded, carefully avoiding disturbing the pellet, and replaced by 800 μl fresh F-buffer. Successful coating was verified using confocal fluorescence microscopy by the presence of a fluorescent ring on the edge of the bead on excitation with a 638 nm laser (Extended Data Fig. 3b). For the other bead type, approximately 50 ng of the generated crosslinker–DNA construct was incubated with 2 μl NeutrAvidin beads in 10 μl F-buffer for 15 min in a rotary mixer at 4 °C, and then rediluted in 500 μl F-buffer with 100 mM biotin excess to block unbound NeutrAvidin. Unbound biotin was removed during the optical tweezer assay by flushing F-buffer after trapping the beads.

Single-molecule data acquisition and analysis. Force spectroscopy data was collected at 500 Hz using custom-built dual-trap optical tweezers and a commercial C-Trap (LUMICKS). Data were analysed using custom scripts in Python v2.7. The optical traps were calibrated using the power spectrum of the Brownian motion of the trapped beads[43], obtaining average stiffness values of $\kappa = 0.39 \pm 0.04$ pN nm^{-1}. After trapping the beads with two different coatings (Extended Data Fig. 3b), α-actinin-4-actin binding was established by approaching and maintaining both beads in close proximity for approximately 10 s. Tether lifetime was assessed by rapidly retracting the beads to a set distance—thus increasing the applied force—and measuring the time until the tether broke. To discriminate single from multiple connections, we used the worm-like chain model and the fact that single double-stranded DNA exhibits an overstretching plateau in the force-extension curve at forces above 65 pN (Extended Data Fig. 3c). We pulled on tethers to high forces and observed that the contour length (computed using the worm-like chain model) of those that displayed an overstretching characteristic of single tethers matched the expected value of 850 nm within an ~60 nm range, probably due to the variability in the bead radii and thickness of the actin coat. Multiple tethers, in contrast to single ones, did not show this characteristic overstretching, and their apparent length was most often shorter (Extended Data Fig. 3c). Therefore, we considered tethers that displayed the expected contour length of 850 ± 30 nm and broke in a clean step. Most tethers showed dissociation below a waiting time of 1 min (55% of tethers across all forces). Tethers that lasted longer generally did not break at all, even after several minutes under tension. Hence, lifetimes were determined from tethers showing dissociation within 1 min.

Reporting summary. Further information on research design is available in the Nature Research Reporting Summary linked to this article.

Data availability

Source data are provided with this paper.

Code availability

The Python script to simulate the minimal 1D crosslinker model can be found at GitHub via https://github.com/YuvalMulla/Minimal_1D_Crosslinker_Model.

References

31. Bell, G. Models for the specific adhesion of cells to cells. *Science* **200**, 618–627 (1978).
32. Pollard, T. D., Blanchoin, L. & Mullins, R. D. Molecular mechanisms controlling actin filament dynamics in nonmuscle cells. *Annu. Rev. Biophys. Biomol. Struct.* **29**, 545–576 (2000).
33. Skrzeszewska, P. J. et al. Fracture and self-healing in a well-defined self-assembled polymer network. *Macromolecules* **43**, 3542–3548 (2010).
34. Jung, W., Murrell, M. P. & Kim, T. F-actin cross-linking enhances the stability of force generation in disordered actomyosin networks. *Comp. Part. Mech.* **2**, 317–327 (2015).
35. Kim, T. Determinants of contractile forces generated in disorganized actomyosin bundles. *Biomech. Model. Mechanobiol.* (2014).
36. Kim, T., Hwang, W., Lee, H. & Kamm, R. D. Computational analysis of viscoelastic properties of crosslinked actin networks. *PLoS Comput. Biol.* **5**, e1000439 (2009).
37. Mak, M., Zaman, M. H., Kamm, R. D. & Kim, T. Interplay of active processes modulates tension and drives phase transition in self-renewing, motor-driven cytoskeletal networks. *Nat. Commun.* **7**, 10323 (2016).
38. Tang, V. W. & Brieher, W. M. α-Actinin-4/FSGS1 is required for Arp2/3-dependent actin assembly at the adherens junction. *J. Cell Biol.* **196**, 115–130 (2012).
39. Schneider, C. A., Rasband, W. S. & Eliceiri, K. W. NIH Image to ImageJ: 25 years of image analysis. *Nat. Methods* **9**, 671–675 (2012).
40. Broedersz, C. P. et al. Cross-link-governed dynamics of biopolymer networks. *Phys. Rev. Lett.* **105**, 238101 (2010).
41. Yin, J. et al. Genetically encoded short peptide tag for versatile protein labeling by Sfp phosphopantetheinyl transferase. *Proc. Natl Acad. Sci. USA* **102**, 15815–15820 (2005).
42. Avellaneda, M. J., Koers, E. J., Minde, D. P., Sunderlikova, V. & Tans, S. J. Simultaneous sensing and imaging of individual biomolecular complexes enabled by modular DNA–protein coupling. *Commun. Chem.* **3**, 20 (2020).
43. Berg-Sørensen, K. & Flyvbjerg, H. Power spectrum analysis for optical tweezers. *Rev. Sci. Instrum.* **75**, 594–612 (2004).

Acknowledgements

We thank M. van Hecke and C. Alkemade for critical reading of the manuscript. We thank P. R. ten Wolde, K. Storm, W. Ellenbroek, C. Broedersz, D. Brueckner and M. Berger for fruitful discussions. We thank W. Brieher and V. Tang from the University of Illinois for the kind gift of purified α-actinin-4 (WT and the K255E point mutant) and their plasmids; M. Kuit-Vinkenoog and J. den Haan for actin and further purification of α-actinin-4; A. Goutou and I. Isturiz-Petitjean for co-sedimentation measurements and V. Sunderlíková for the design, mutagenesis, cloning and purifying of the α-actinin-4 constructs used in the single-molecule experiments. We gratefully acknowledge financial support from the following sources: research program of the Netherlands Organization for Scientific Research (NWO) (S.J.T., A.R. and M.J.A.); ERC Starting Grant (335672-MINICELL) (G.H.K. and Y.M.). 'BaSyC—Building a Synthetic Cell' Gravitation grant (024.003.019) of the Netherlands Ministry of Education, Culture and Science (OCW) and the Netherlands Organisation for Scientific Research (G.H.K. and L.B.); and support from the National Institutes of Health (1R01GM126256) (T.K. and W.J.).

Author contributions

Y.M. and G.H.K. conceived and designed the study. M.J.A. and S.J.T. designed the optical tweezer experiments. M.J.A., A.R. and L.B. performed the optical tweezer experiments. M.J.A. and A.R. analysed the optical tweezer experiments. Y.M. performed and analysed all the other experiments and designed and simulated the 1D model. W.J. and T.K. designed, performed and analysed the actin network simulations. Y.M., M.J.A., T.K., S.J.T. and G.H.K. wrote the manuscript with input from W.J., A.R. and L.B. All the authors approved the final version.

Competing interests

The authors declare no competing interests.

Additional information

Extended data is available for this paper at https://doi.org/10.1038/s41563-022-01288-0.

Supplementary information The online version contains supplementary material available at https://doi.org/10.1038/s41563-022-01288-0.

Correspondence and requests for materials should be addressed to Taeyoon Kim, Sander J. Tans or Gijsje H. Koenderink.

Peer review information *Nature Materials* thanks Patricia Bassereau, Jean-Francois Joanny and the other, anonymous, reviewer(s) for their contribution to the peer review of this work.

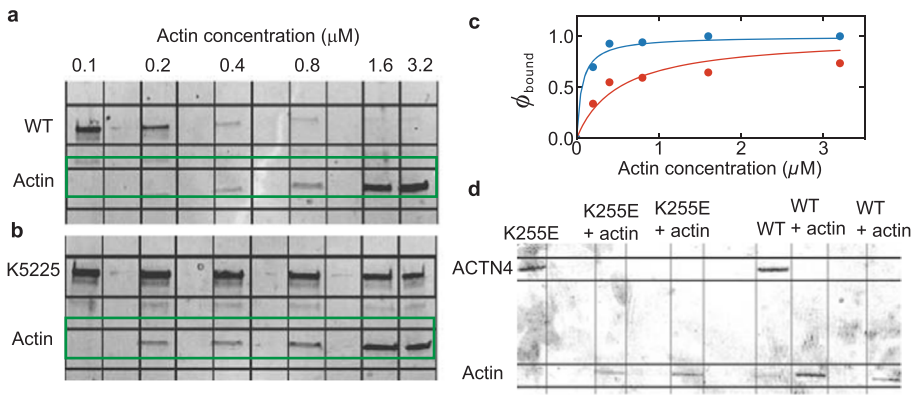

Extended Data Fig. 1 | High-speed co-sedimentation measurements of the affinity of α-actinin-4 (WT) and K255E crosslinkers for actin filaments. **a, b**, supernatant resulting from a high-speed centrifugation of a mixture of actin filaments and crosslinkers was run on an SDS-page gel. The bands on the bottom show the α-actinin-4 (WT) or K255E (resp. **a** and **b**, molecular weight ~ 100 kDa in both cases), while the bands on the top show actin (42 kDa). Each labelled column contained a different actin concentration as indicated. Some lanes were kept empty as spacers. The crosslinker concentration was fixed at 0.1 μM. A single measurement was performed per condition. **c**, The fraction of bound crosslinkers, as determined from the co-sedimentation assay, as a function of the actin concentration was fit to the equation: $\varphi_{bound} = \frac{c_{actin}}{K_a}$, where K_a is the affinity of the crosslinker. **d**, Consistent with the high affinity of both crosslinkers, SDS-page gels of supernatant resulting from a high-speed centrifugation of a crosslinked actin network at the concentration used in all our experiments (48 μM actin together with 0.48 μM crosslinker) do not show any measurable fraction of unbound crosslinkers. A single measurement was performed per condition.

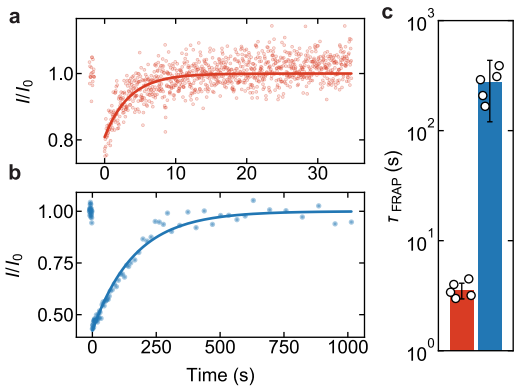

Extended Data Fig. 2 | Fluorescence recovery after photobleaching measurements reveal that α-actinin-4 crosslinkers are more dynamic than the K255E mutant. Example fluorescence recovery curves of α-actinin-4 (**a**) and K255E (**b**) in the presence of 48 μM actin show full recovery of both proteins after photobleaching at time t=0, but with different timescales. The solid lines represent exponential fits to the data (see Methods). **c**, Average recovery time for α-actinin-4 (red) and for K255E (blue), with the standard error on basis of 5 measurements of different locations within the same sample per condition. Measurements were performed at 25 °C.

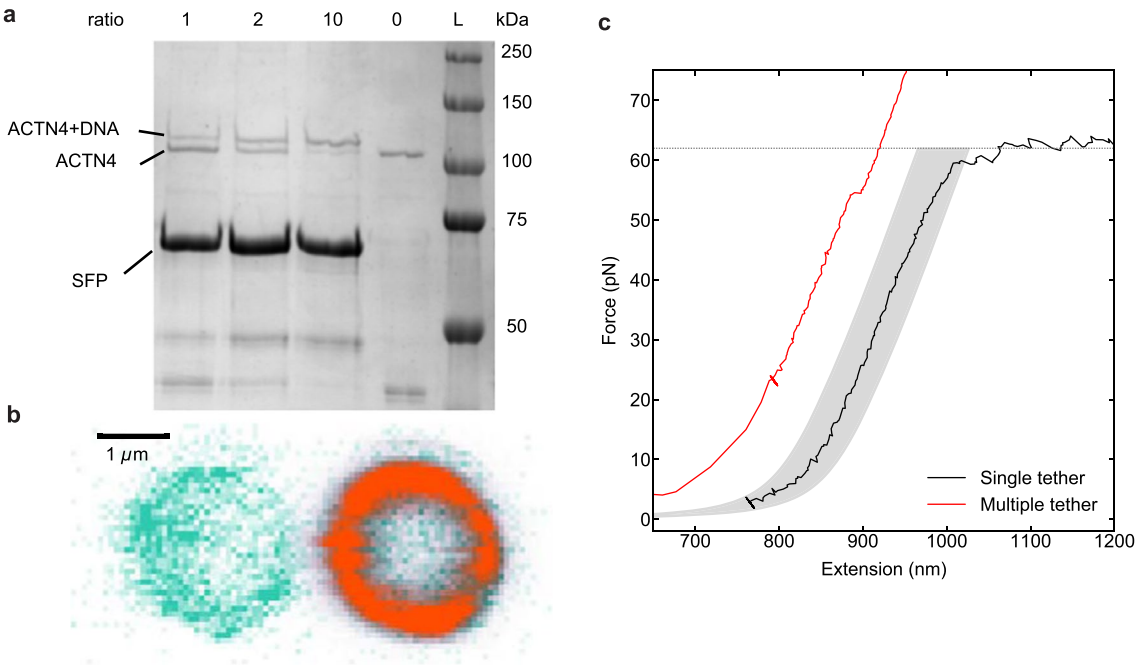

Extended Data Fig. 3 | Generation and classification of α-actinin-4/actin tethers. a, DNA was coupled to α-actinin-4 (WT or K255E) using an SFP synthase-mediated reaction. Because α-actinin-4 is a homodimer, the yBBr tag used for coupling is present in both monomers. To favour DNA attachment to only one monomer, we performed coupling reactions with several DNA titrations, and the coupling yields were quantified using SDS-PAGE gel electrophoresis. The DNA:α-actinin-4 molar ratios are indicated above each lane. At a molar ratio of 1:1, most of the α-actinin-4 is uncoupled, that is most dimers will be either not coupled or have only one monomer coupled to DNA. A single measurement was performed per condition. **b**, Concurrent confocal fluorescence images of a trapped bead coated with α-actinin-4 (left) and a trapped bead coated with actin filaments (right). The bead's autofluorescence is depicted in green, and the fluorescent emission of Alexa Fluor 647-tagged actin is depicted in orange. In total, 36 images have been taken of 4 independent samples. This image shows representative examples. **c**, Force-extension curves showing the overstretching regime of a single dsDNA tether (black), and a case where the two beads are linked by multiple tethers, which yields a shorter contour length and higher forces without unzipping (red). Variability in bead radii and actin layer thickness results in force-extension curves that can be shifted along the Extension axis, from the theoretical 850 nm by ±30 nm. Grey area:'single-tether region'. Tethers with a force-extension curve within this area that broke in a single step were regarded as single tethers and hence included in measuring the force-dependent lifetime.

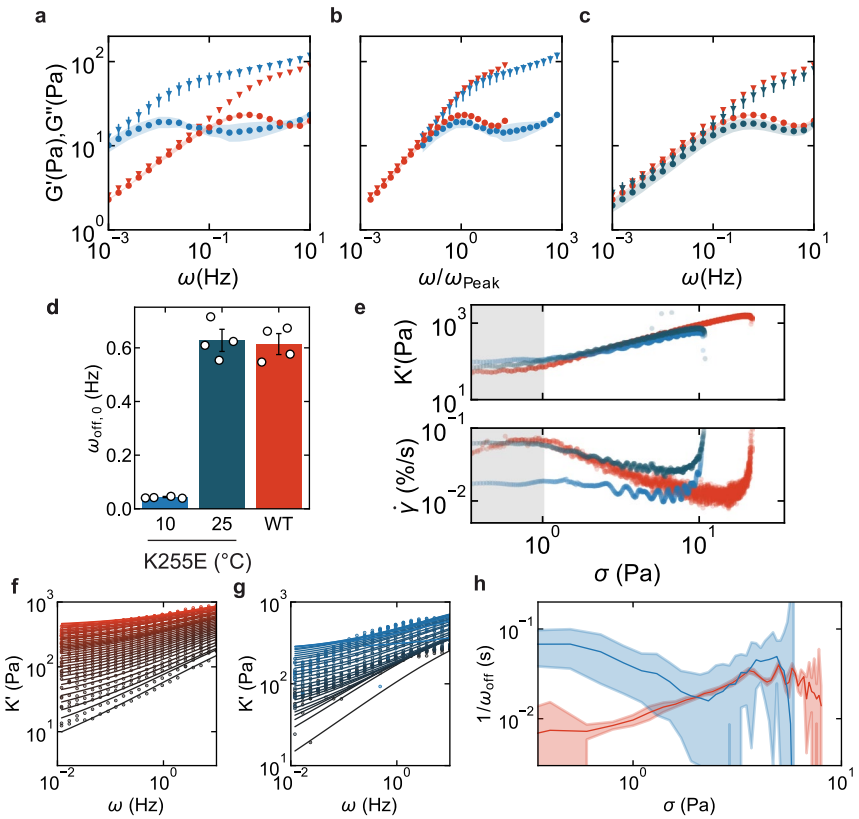

Extended Data Fig. 4 | Nonlinear and temperature-dependent rheology of actin networks crosslinked by α-actinin-4 or K255E. Rheological measurements of wild type (red) and K255E mutant (light blue) α-actinin-4 crosslinking actin networks at 10 °C and of K255E mutant crosslinked actin networks at 25 °C (dark blue). **a-c**, The storage (triangles) and loss moduli (circles) were measured using small amplitude oscillatory shear. The moduli are shown as a function of frequency (**a**) and as a function of the frequency normalized by the frequency at which the loss modulus peaks (**b**). Both curves are measured at 10 °C. Data are presented as mean values +/- the standard error indicated by bars and shaded regions on basis of 4 independent samples per condition. The collapses in **b** and **c** show that the crosslinker unbinding kinetics, but not the network structure, is significantly different for the different conditions (see Main Text). **d**, The stress relaxation frequency was extracted from Extended Data Fig. 4a, c using Methods equations 4–7. Data are presented as mean values +/- the standard error on basis of 4 independent samples per condition. **e**, Representative example curves of the differential storage modulus at 0.5 Hz (top) and of the strain rate (bottom) are plotted against the applied shear stress. We define the rupture strain as the data point where K′ peaks. **f-g**, We apply a semiflexible polymer network model to fit the frequency-dependent differential elastic modulus as a function of prestress (see Methods). **h**, Thus, we extract the crosslinker bound lifetime as a function of stress for both α-actinin-4 (red) and the K255E mutant (blue) at 25 °C. The shaded areas represent the error on basis of the fits. The bound lifetime of the mutant is significantly longer at low stress, but the lifetimes of both types become similar at high stress as the bound lifetime of the wild type increases. The abrupt decay of bound lifetime in the K255E-crosslinked network when the stress reaches 5 Pa is due to network fracturing.

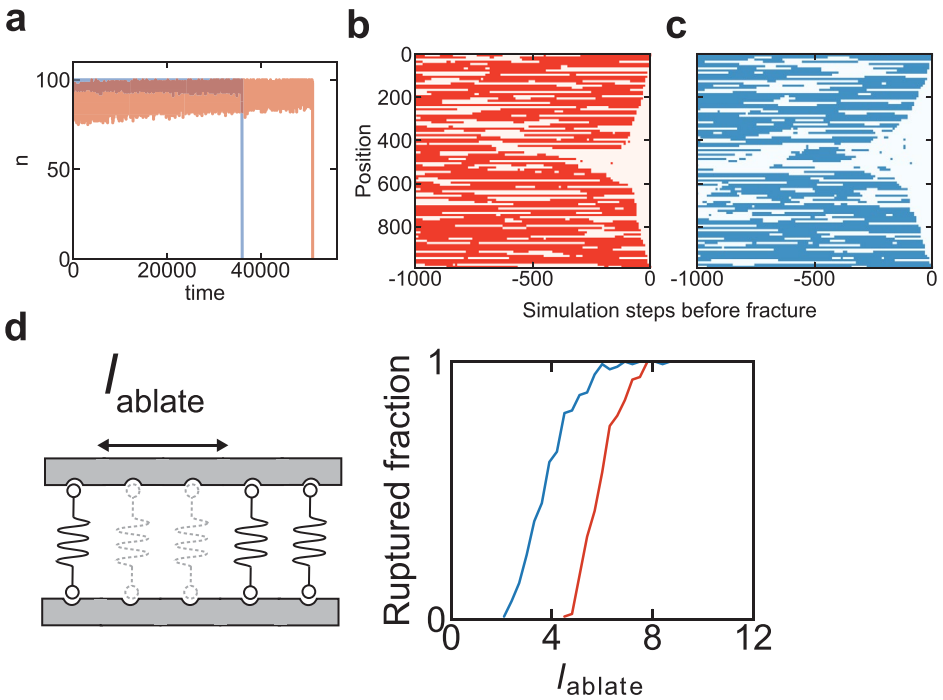

Extended Data Fig. 5 | Fracturing in the minimal 1D crosslinker model. a, Time trace of the bound number of catch bonds (red) and slip bonds (blue) in a network undergoing a linearly increasing stress (see Supplementary Table 1 for parameters). As the catch bonds have faster dynamics than the slip bonds, a larger spread in the bound fraction is observed. After a long time of steady state fluctuations, the networks suddenly fracture as the number of linkers rapidly goes to 0. **b, c**, Kymographs showing at which positions there are bonds (red for catch bonds, blue for slip bonds) or no bonds (white). At steady state, linkers continuously bind and unbind (−1000 to approximately −300 steps). Cracks can spontaneously initiate and propagate through the network (the last ~300 steps of the simulation) for both catch and slip bonds in a similar manner. **d**, The fraction of 1D-networks that rupture when a gap of varying ablation length l_{ablate} is introduced for both catch (red) and slip bonds (blue). Inset: schematic of the ablation simulation.

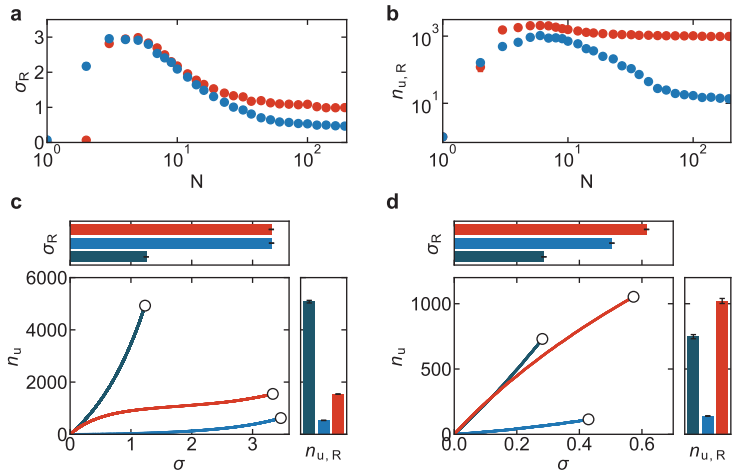

Extended Data Fig. 6 | Simulations show that catch bonds only provide a mechanical advantage over slip bonds when they are mobile and present in sufficiently large numbers. The system size dependence of the rupture stress (**a**) and bond turnover at the point of rupture (**b**) reveals that catch bonds (red) are only stronger than slip bonds (blue) for networks larger than ~10 bonds, emphasizing that the increased network strength by catch bonding is an emergent property (Supplementary Note 1). Each data point is the average of 10 repeats and the standard errors are smaller than the symbol size. **c**, Catch bond-induced network strengthening is not observed when crosslinkers are immobile and rebind in the same location from which they unbound. The bond turnover as a function of stress reveals catch bonds (red) cause more dynamic materials (right), but do not enhance strength (top) compared to strong slip bonds (light blue) and are less dynamic than networks consisting of weak slip bonds (dark blue). Data are presented as mean values +/- the standard error on basis of 100 independent simulation runs per condition. **d**, We also considered a three-state model where linkers are doubly bound, singly bound or unbound (Supplementary Note 1). Similar to the two-state model, the bond turnover as a function of stress reveals that networks of catch bonds (red) are stronger and more deformable than networks of strong slip bonds (light blue) or weak slip bonds (dark blue). Data are presented as mean values +/- the standard error on basis of 5 independent simulation runs per condition.

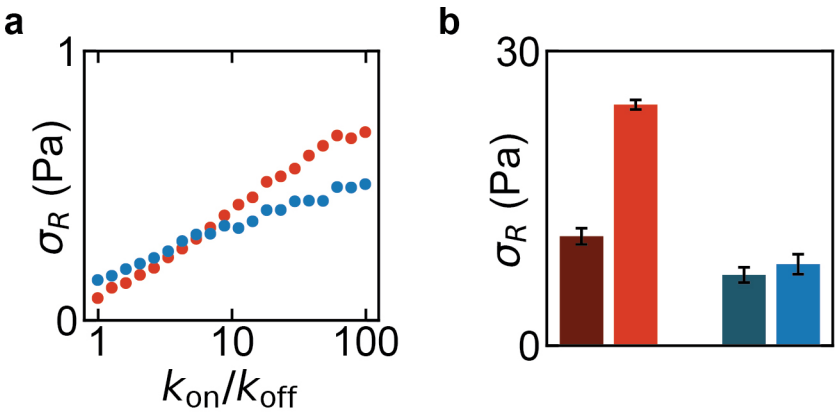

Extended Data Fig. 7 | Catch bonding is only effective when the bond lifetime is high. a, Simulations of the rupture stress as a function of the bond lifetime $k_{on}/k_{off,0}^{slip}$, keeping $k_{off,0}^{slip}/k_{off,0}^{catch}$ fixed (see Methods and Supplementary Table 1), shows that catch bonds (red) are only stronger than slip bonds (blue) when the binding rate is high. **b**, Consistent with the simulations, enhancing the bond lifetime in experiments by decreasing the temperature from 25 °C (light) to 10 °C (dark) increases the rupture stress more steeply for wild type α-actinin-4 (red) than for K255E (blue). The error bars represent the standard error (N=4 independent samples for each condition).

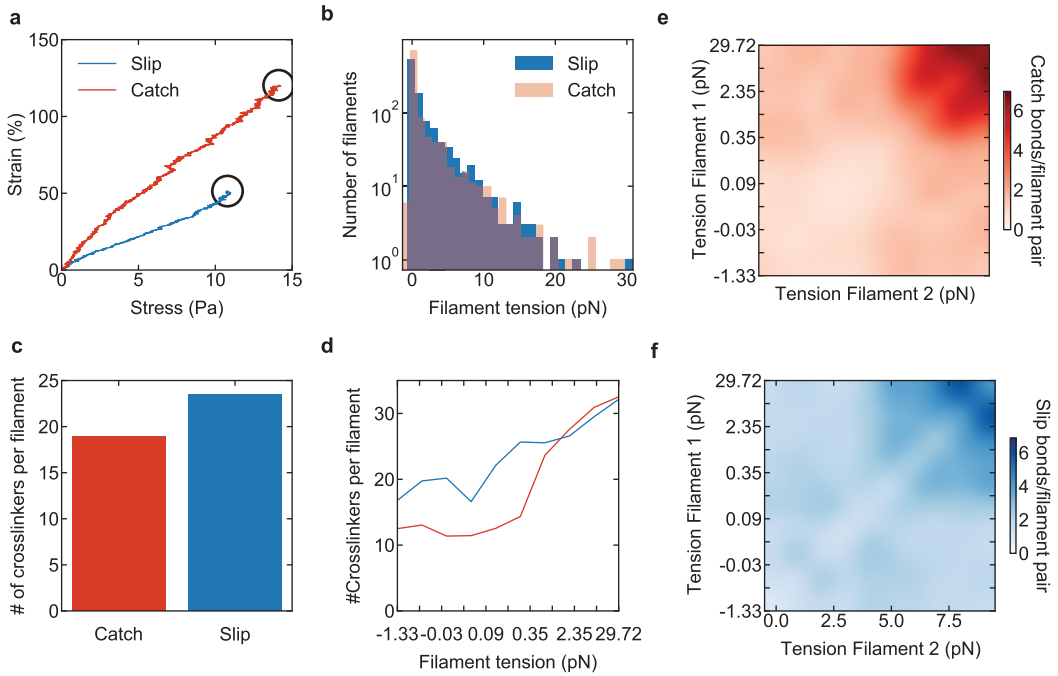

Extended Data Fig. 8 | Actin network simulations. a, Stress-strain curve of the simulated catch (red) and slip bond (blue) actin networks. The black circles indicate the yielding points of both networks (see Methods). **b**, Distribution of tension on actin filaments in networks for simulated catch bond (red) and slip bond (blue) with 10 Pa stress. **c**, The polymer network simulation predicts that the average number of active crosslinkers per filament at 10 Pa is lower for catch bonds than for slip bonds, in line with the 1D simulations (panel a) and the catch bond's lower bond lifetime. **d**, The average number of crosslinkers as a function of the filament tension shows that slip bonds are mainly enriched on low-tension filaments. The tension on the x-axis is binned such that each bin contains 10% of the filaments. **e-f**, Similar plots as Fig. 3d but then for the catch (d, red) and slip bond (e, blue) simulations separately: the active crosslinkers are binned according to tension acting on pairs of filaments (tension on filament 1 on x-axis, tension on filament 2 on y-axis) connected by the crosslinkers. 10×10 bins are used, and the distribution was smoothed using bicubic interpolation. The tension spacing along the x- and y-axis is non-uniform, such that each bin includes 10% of the filaments. These plots show that both catch and slip bonds preferentially connect tense filaments, likely because of geometrical reasons and/or because filament tension resulted from having more crosslinkers bound. However, catch bonds localize more strongly to tense filaments than slip bonds (Fig. 3d) because they bind less to the rest of the network due to their higher off-rate in the absence of force and therefore redistribute to the tense filaments (Fig. 3e).

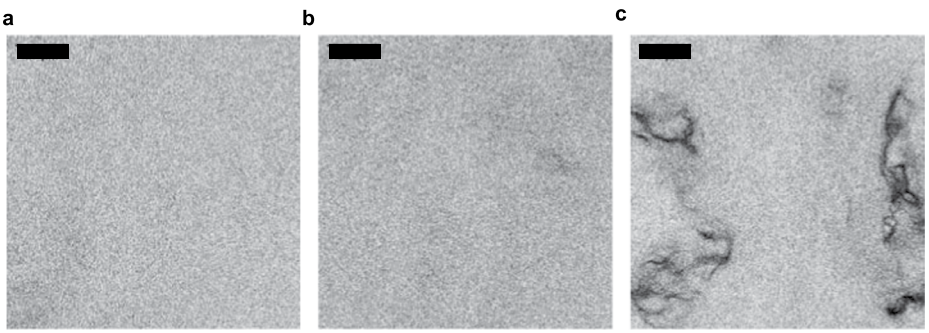

Extended Data Fig. 9 | Confocal fluorescence images of crosslinked actin networks. 10% of the actin monomers were labelled with Alexafluor-647. At a 1:100 crosslinker:actin molar ratio, the actin networks studied in this work are isotropic and spatially uniform, for both wild type (**a**) and K255E α-actinin-4 (**b**). We do not observe any discernable structure because the mesh size is ~200 nm, which is on the order of the diffraction limit, indicating that filaments are isotropically crosslinked rather than bundled. **c**, For comparison, actin bundle clusters were observed at a 1:25 α-actinin-4:actin molar ratio. The colour coding was inverted for all images to improve the visual contrast between bundles and background. Scale bars are 20 μm. 10 images were taken of different locations within the same sample per condition and all images had similar results per condition.

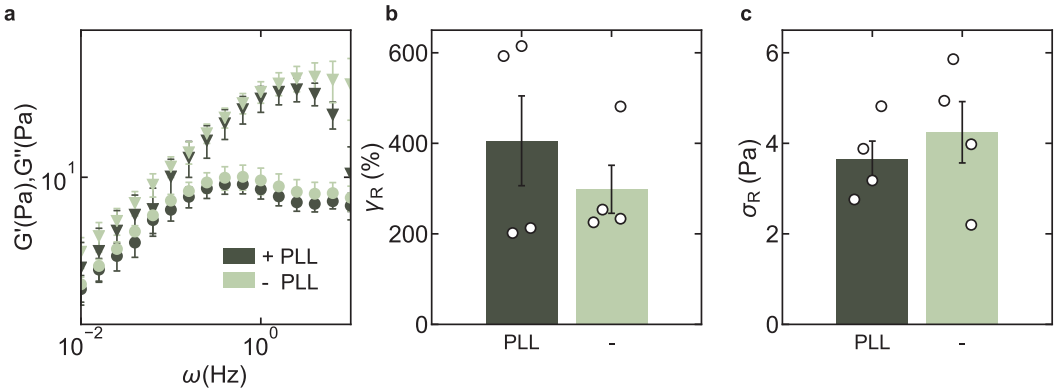

Extended Data Fig. 10 | Fracturing occurs within the actin network, not at the rheometer-network interface. The rheology of wild type α-actinin-crosslinked actin networks was compared in the presence (dark green) or absence (light green) of a Polylysine-coated surface on both the bottom and top plate of the rheometer (see Methods). **a)** a frequency sweep at zero prestress shows that the linear rheology is unaffected by changing the rheometer-network interface. The storage (triangles) and loss moduli (circles) were measured as a function of frequency using small amplitude oscillatory shear. **b)** the network rupture strain and **c)** rupture stress (bottom) are not significantly affected by the addition of Polylysine at the rheometer-network interface. The error bars represent the standard error (N=4 independent samples for each condition).

nature portfolio

Corresponding author(s): Gijsje Koenderink, Sander Tans, Taeyoon Kim

Last updated by author(s): 10/02/2022

Reporting Summary

Nature Portfolio wishes to improve the reproducibility of the work that we publish. This form provides structure for consistency and transparency in reporting. For further information on Nature Portfolio policies, see our Editorial Policies and the Editorial Policy Checklist.

Statistics

For all statistical analyses, confirm that the following items are present in the figure legend, table legend, main text, or Methods section.

n/a	Confirmed	
☐	☒	The exact sample size (*n*) for each experimental group/condition, given as a discrete number and unit of measurement
☐	☒	A statement on whether measurements were taken from distinct samples or whether the same sample was measured repeatedly
☒	☐	The statistical test(s) used AND whether they are one- or two-sided *Only common tests should be described solely by name; describe more complex techniques in the Methods section.*
☒	☐	A description of all covariates tested
☐	☒	A description of any assumptions or corrections, such as tests of normality and adjustment for multiple comparisons
☐	☒	A full description of the statistical parameters including central tendency (e.g. means) or other basic estimates (e.g. regression coefficient) AND variation (e.g. standard deviation) or associated estimates of uncertainty (e.g. confidence intervals)
☒	☐	For null hypothesis testing, the test statistic (e.g. *F*, *t*, *r*) with confidence intervals, effect sizes, degrees of freedom and *P* value noted *Give P values as exact values whenever suitable.*
☒	☐	For Bayesian analysis, information on the choice of priors and Markov chain Monte Carlo settings
☒	☐	For hierarchical and complex designs, identification of the appropriate level for tests and full reporting of outcomes
☒	☐	Estimates of effect sizes (e.g. Cohen's *d*, Pearson's *r*), indicating how they were calculated

Our web collection on statistics for biologists contains articles on many of the points above.

Software and code

Policy information about availability of computer code

Data collection	The Python script to simulate the minimal 1D crosslinker model can be found at https://github.com/YuvalMulla/Minimal_1D_Crosslinker_Model.
Data analysis	ImageJ v1.52i was used for image analysis in Extended Data Fig. 1.

For manuscripts utilizing custom algorithms or software that are central to the research but not yet described in published literature, software must be made available to editors and reviewers. We strongly encourage code deposition in a community repository (e.g. GitHub). See the Nature Portfolio guidelines for submitting code & software for further information.

Data

Policy information about availability of data

All manuscripts must include a data availability statement. This statement should provide the following information, where applicable:

- Accession codes, unique identifiers, or web links for publicly available datasets
- A description of any restrictions on data availability
- For clinical datasets or third party data, please ensure that the statement adheres to our policy

The source data of all Main and Extended Data Figures is provided in this manuscript.

Field-specific reporting

Please select the one below that is the best fit for your research. If you are not sure, read the appropriate sections before making your selection.

☒ Life sciences ☐ Behavioural & social sciences ☐ Ecological, evolutionary & environmental sciences

For a reference copy of the document with all sections, see nature.com/documents/nr-reporting-summary-flat.pdf

Life sciences study design

All studies must disclose on these points even when the disclosure is negative.

Sample size	Sample sizes are always reported in the captions and/or methods section. No sample size calculation was performed before the experiments. Instead, the samples sizes were based on similar previous experiments.
Data exclusions	No data was excluded from the studies.
Replication	Reproducibility of results was ensured by replicate experiments, all replicate experiments are included in the manuscript.
Randomization	No randomization was performed in this study.
Blinding	No blinding was performed in this study.

Reporting for specific materials, systems and methods

We require information from authors about some types of materials, experimental systems and methods used in many studies. Here, indicate whether each material, system or method listed is relevant to your study. If you are not sure if a list item applies to your research, read the appropriate section before selecting a response.

Materials & experimental systems

n/a	Involved in the study
☒	☐ Antibodies
☒	☐ Eukaryotic cell lines
☒	☐ Palaeontology and archaeology
☒	☐ Animals and other organisms
☒	☐ Human research participants
☒	☐ Clinical data
☒	☐ Dual use research of concern

Methods

n/a	Involved in the study
☒	☐ ChIP-seq
☒	☐ Flow cytometry
☒	☐ MRI-based neuroimaging